First Measurement of the Tensor Structure Function b_1 of the Deuteron.

A. Airapetian,[31] N. Akopov,[31] Z. Akopov,[31] M. Amarian,[8,31] V.V. Ammosov,[23] A. Andrus,[16] E.C. Aschenauer,[8] W. Augustyniak,[30] R. Avakian,[31] A. Avetissian,[31] E. Avetissian,[12] P. Bailey,[16] D. Balin,[22] V. Baturin,[22] M. Beckmann,[7] S. Belostotski,[22] S. Bernreuther,[10] N. Bianchi,[12] H.P. Blok,[21,29] H. Böttcher,[8] A. Borissov,[18] A. Borysenko,[12] M. Bouwhuis,[16] J. Brack,[6] A. Brüll,[17] V. Bryzgalov,[23] G.P. Capitani,[12] T. Chen,[4] H.C. Chiang,[16] G. Ciullo,[11] M. Contalbrigo,[11] P.F. Dalpiaz,[11] R. De Leo,[3] M. Demey,[21] L. De Nardo,[1] E. De Sanctis,[12] E. Devitsin,[19] P. Di Nezza,[12] J. Dreschler,[21] M. Düren,[14] M. Ehrenfried,[10] A. Elalaoui-Moulay,[2] G. Elbakian,[31] F. Ellinghaus,[8] U. Elschenbroich,[13] R. Fabbri,[21] A. Fantoni,[12] A. Fechtchenko,[9] L. Felawka,[27] B. Fox,[6] S. Frullani,[25] G. Gapienko,[23] V. Gapienko,[23] F. Garibaldi,[25] K. Garrow,[1,26] E. Garutti,[21] D. Gaskell,[6] G. Gavrilov,[7,27] V. Gharibyan,[31] G. Graw,[20] O. Grebeniouk,[22] L.G. Greeniaus,[1,27] I.M. Gregor,[8] K. Hafidi,[2] M. Hartig,[27] D. Hasch,[12] D. Heesbeen,[21] M. Henoch,[10] R. Hertenberger,[20] W.H.A. Hesselink,[21,29] A. Hillenbrand,[10] M. Hoek,[14] Y. Holler,[7] B. Hommez,[13] G. Iarygin,[9] A. Ivanilov,[23] A. Izotov,[22] H.E. Jackson,[2] A. Jgoun,[22] R. Kaiser,[15] E. Kinney,[6] A. Kisselev,[22] M. Kopytin,[8] V. Korotkov,[23] V. Kozlov,[19] B. Krauss,[10] V.G. Krivokhijine,[9] L. Lagamba,[3] L. Lapikás,[21] A. Laziev,[21,29] P. Lenisa,[11] P. Liebing,[8] L.A. Linden-Levy,[16] K. Lipka,[8] W. Lorenzon,[18] H. Lu,[5] J. Lu,[27] S. Lu,[14] B.-Q. Ma,[4] B. Maiheu,[13] N.C.R. Makins,[16] Y. Mao,[4] B. Marianski,[30] H. Marukyan,[31] F. Masoli,[11] V. Mexner,[21] N. Meyners,[7] O. Mikloukho,[22] C.A. Miller,[1,27] Y. Miyachi,[28] V. Muccifora,[12] A. Nagaitsev,[9] E. Nappi,[3] Y. Naryshkin,[22] A. Nass,[10] M. Negodaev,[8] W.-D. Nowak,[8] K. Oganessyan,[7,12] H. Ohsuga,[28] N. Pickert,[10] S. Potashov,[19] D.H. Potterveld,[2] M. Raithel,[10] D. Reggiani,[11] P.E. Reimer,[2] A. Reischl,[21] A.R. Reolon,[12] C. Riedl,[10] K. Rith,[10] G. Rosner,[15] A. Rostomyan,[31] L. Rubacek,[14] J. Rubin,[16] D. Ryckbosch,[13] Y. Salomatin,[23] I. Sanjiev,[2,22] I. Savin,[9] A. Schäfer,[24] C. Schill,[12] G. Schnell,[8,28] K.P. Schüler,[7] J. Seele,[16] R. Seidl,[10] B. Seitz,[14] R. Shanidze,[10] C. Shearer,[15] T.-A. Shibata,[28] V. Shutov,[9] M.C. Simani,[21,29] K. Sinram,[7] M. Stancari,[11] M. Statera,[11] E. Steffens,[10] J.J.M. Steijger,[21] H. Stenzel,[14] J. Stewart,[8] F. Stinzing,[10] U. Stösslein,[6] P. Tait,[10] H. Tanaka,[28] S. Taroian,[31] B. Tchuiko,[23] A. Terkulov,[19] A. Tkabladze,[13] A. Trzcinski,[30] M. Tytgat,[13] A. Vandenbroucke,[13] P.B. van der Nat,[21,29] G. van der Steenhoven,[21] M.C. Vetterli,[26,27] V. Vikhrov,[22] M.G. Vincter,[1] C. Vogel,[10] M. Vogt,[10] J. Volmer,[8] C. Weiskopf,[10] J. Wendland,[26,27] J. Wilbert,[10] Y. Ye,[5] Z. Ye,[7] S. Yen,[27] B. Zihlmann,[21] and P. Zupranski[30]

(The HERMES Collaboration)

[1]*Department of Physics, University of Alberta, Edmonton, Alberta T6G 2J1, Canada*
[2]*Physics Division, Argonne National Laboratory, Argonne, Illinois 60439-4843, USA*
[3]*Istituto Nazionale di Fisica Nucleare, Sezione di Bari, 70124 Bari, Italy*
[4]*School of Physics, Peking University, Beijing 100871, China*
[5]*Department of Modern Physics, University of Science and Technology of China, Hefei, Anhui 230026, China*
[6]*Nuclear Physics Laboratory, University of Colorado, Boulder, Colorado 80309-0390, USA*
[7]*DESY, 22603 Hamburg, Germany*
[8]*DESY, 15738 Zeuthen, Germany*
[9]*Joint Institute for Nuclear Research, 141980 Dubna, Russia*
[10]*Physikalisches Institut, Universität Erlangen-Nürnberg, 91058 Erlangen, Germany*
[11]*Istituto Nazionale di Fisica Nucleare, Sezione di Ferrara and Dipartimento di Fisica, Università di Ferrara, 44100 Ferrara, Italy*
[12]*Istituto Nazionale di Fisica Nucleare, Laboratori Nazionali di Frascati, 00044 Frascati, Italy*
[13]*Department of Subatomic and Radiation Physics, University of Gent, 9000 Gent, Belgium*
[14]*Physikalisches Institut, Universität Gießen, 35392 Gießen, Germany*
[15]*Department of Physics and Astronomy, University of Glasgow, Glasgow G12 8QQ, United Kingdom*
[16]*Department of Physics, University of Illinois, Urbana, Illinois 61801-3080, USA*
[17]*Laboratory for Nuclear Science, Massachusetts Institute of Technology, Cambridge, Massachusetts 02139, USA*
[18]*Randall Laboratory of Physics, University of Michigan, Ann Arbor, Michigan 48109-1040, USA*
[19]*Lebedev Physical Institute, 117924 Moscow, Russia*
[20]*Sektion Physik, Universität München, 85748 Garching, Germany*
[21]*Nationaal Instituut voor Kernfysica en Hoge-Energiefysica (NIKHEF), 1009 DB Amsterdam, The Netherlands*
[22]*Petersburg Nuclear Physics Institute, St. Petersburg, Gatchina, 188350 Russia*
[23]*Institute for High Energy Physics, Protvino, Moscow region, 142281 Russia*
[24]*Institut für Theoretische Physik, Universität Regensburg, 93040 Regensburg, Germany*
[25]*Istituto Nazionale di Fisica Nucleare, Sezione Roma 1, Gruppo Sanità and Physics Laboratory, Istituto Superiore di Sanità, 00161 Roma, Italy*
[26]*Department of Physics, Simon Fraser University, Burnaby, British Columbia V5A 1S6, Canada*
[27]*TRIUMF, Vancouver, British Columbia V6T 2A3, Canada*

[28] Department of Physics, Tokyo Institute of Technology, Tokyo 152, Japan
[29] Department of Physics and Astronomy, Vrije Universiteit, 1081 HV Amsterdam, The Netherlands
[30] Andrzej Soltan Institute for Nuclear Studies, 00-689 Warsaw, Poland
[31] Yerevan Physics Institute, 375036 Yerevan, Armenia

(Dated: October 10, 2005)

The HERMES experiment has investigated the tensor spin structure of the deuteron using the 27.6 GeV/c positron beam of HERA. The use of a tensor polarized deuteron gas target with only a negligible residual vector polarization enabled the first measurement of the tensor asymmetry A_{zz}^{d} and the tensor structure function b_1^{d} for average values of the Bjørken variable $0.01 < \langle x \rangle < 0.45$ and of the negative of the squared four-momentum transfer $0.5\ \mathrm{GeV}^2 < \langle Q^2 \rangle < 5\ \mathrm{GeV}^2$. The quantities A_{zz}^{d} and b_1^{d} are found to be non-zero. The rise of b_1^{d} for decreasing values of x can be interpreted to originate from the same mechanism that leads to nuclear shadowing in unpolarized scattering.

PACS numbers: 13.60.-r, 13.88.+e, 14.20.Dh, 14.65.-q

Inclusive deep-inelastic scattering (DIS) of charged leptons from the deuteron, a spin-1 object, is described by eight structure functions, twice as many as required to describe DIS from a spin-1/2 nucleon [1]. The three leading-twist structure functions relevant to this discussion can be written within the Quark-Parton Model as:

	Nucleon	Deuteron
F_1	$\frac{1}{2}\sum_q e_q^2\,[q_\uparrow^{\frac{1}{2}} + q_\uparrow^{-\frac{1}{2}}]$	$\frac{1}{3}\sum_q e_q^2\,[q_\uparrow^{1} + q_\uparrow^{-1} + q_\uparrow^{0}]$
g_1	$\frac{1}{2}\sum_q e_q^2\,[q_\uparrow^{\frac{1}{2}} - q_\downarrow^{\frac{1}{2}}]$	$\frac{1}{2}\sum_q e_q^2\,[q_\uparrow^{1} - q_\downarrow^{1}]$
b_1	$--$	$\frac{1}{2}\sum_q e_q^2\left[2q_\uparrow^0 - (q_\uparrow^1 + q_\uparrow^{-1})\right]$.

where $q_\uparrow^m (q_\downarrow^m)$ is the number density of quarks with spin up(down) along the z axis in a hadron(nucleus) with helicity m moving with infinite momentum along the z axis. Reflection symmetry implies that $q_\uparrow^m = q_\downarrow^{-m}$. The sums run over quark and antiquark flavors q with a charge e_q in units of the elementary charge e. Both structure functions and quark number densities depend on the Bjørken variable x which can be interpreted as the fraction of the nucleon momentum carried by the struck quark in the infinite-momentum frame, and $-Q^2$, the square of the four-momentum transfer by the virtual photon.

The polarization-averaged structure function F_1 describes the quark distributions averaged over the target spin states. The polarization-dependent structure function g_1 describes the imbalance in the distribution of quarks with the same $q_\uparrow^m$ or opposite $q_\downarrow^m$ helicity with respect to that of the parent hadron. It can be measured only when both beam and target are polarized. The tensor structure function b_1 does not exist for spin-1/2 targets and vanishes in the absence of nuclear effects, i.e. if the deuteron simply consists of a proton and neutron in a relative S-state. It describes the difference in the quark distributions between the helicity-0, $q^0 = (q_\uparrow^0 + q_\downarrow^0) = 2q_\uparrow^0$, and the averaged non-zero helicity, $q^1 = (q_\uparrow^1 + q_\downarrow^1) = (q_\uparrow^1 + q_\uparrow^{-1})$, states of the deuteron [1–3]. Because b_1 depends only on the spin averaged quark distributions $b_1 = \frac{1}{2}\sum_q e_q^2\left[q^0 - q^1\right]$, its measurement does not require a polarized beam. Since the magnitude of b_1^{d} was expected to be small, it was usually ignored in the extraction of g_1^{d} and, as a consequence, of the neutron structure function g_1^{n} derived from deuteron and proton data. This is in general not *a priori* justified. This paper reports the first measurement of b_1^{d}, performed by the HERMES collaboration using a data set taken with a positron beam and a tensor-polarized deuterium target, and an integrated luminosity of 42 pb^{-1}.

The HERMES experiment [4] was designed to investigate the internal spin structure of nucleons and nuclei by deep-inelastic scattering of polarized positrons and electrons by polarized gaseous targets (e.g. hydrogen, deuterium and helium–3) internal to the HERA-e storage ring. The positrons (electrons) circulating in the ring become transversely polarized by the emission of spin-flip synchrotron radiation [5]. A longitudinal beam polarization is generated at HERMES by the use of a pair of spin rotators before and after the experiment. Beam polarization is employed for the simultaneous g_1^{d} measurement and for studies on beam related systematic effects on b_1^{d}.

A feature of HERMES unique among polarized DIS experiments is its atomic-gas target that is not diluted by non-polarizable material [6]. The target cell is an open-ended elliptical aluminum tube internal to the beam line (40 cm long, 75 μm in wall thickness), which is used to confine the polarized gas along the beam. A magnetic field surrounding the target and aligned with the beam provides the quantization axis for the nuclear spin. A sample of gas was continuously drawn from the cell and analyzed to determine the atomic and molecular abundances and the nuclear polarization of the atoms. An atomic beam source (ABS) generates a deuterium atomic beam and selects the two hyperfine states with the desired nuclear polarization to be injected into the cell. This system allows the selection of substates with pure tensor polarization $P_{zz} = (n^+ + n^- - 2n^0)/(n^+ + n^- + n^0)$ and at the same time vanishing vector polarization $P_z = (n^+ - n^-)/(n^+ + n^- + n^0)$, a combination which is not possible for solid-state polarized targets. Here n^+, n^-, n^0 are the atomic populations with positive, negative and zero spin projection on the beam direction, respectively. Every 90 seconds the polarization of the injected gas is changed; for the $b_1^{\rm d}$ measurement the four injection modes listed in Table I were continuously cycled. Note that the vector$^+$ and vector$^-$ modes are also employed for the $g_1^{\rm d}$ measurement.

The HERMES detector [4] is a forward spectrometer with a dipole magnet providing a field integral of 1.3 Tm. A horizontal iron plate shields the HERA beam lines from this field, thus dividing the spectrometer into two identical halves with ±170 mrad horizontal and ±40 to ±140 mrad vertical acceptance for the polar scattering angle. Tracking is based on 36 drift chamber planes in each detector-half. Positron identification is accomplished using a likelihood method based on signals of four subsystems: a ring-imaging Čerenkov detector, a lead-glass calorimeter, a transition-radiation detector, and a preshower hodoscope. For positrons in the momentum range of 2.5 GeV/c to 27 GeV/c, the identification efficiency exceeds 98% and the hadron contamination is less than 0.5%. The average polar angle resolution is 0.6 mrad and the average momentum resolution is 2%.

For a target state characterized by P_z and P_{zz}, the DIS yield measured by the experiment is proportional to the double differential cross section of polarized DIS

$$\frac{{\rm d}^2\sigma_P}{{\rm d}x{\rm d}Q^2} \simeq \frac{{\rm d}^2\sigma}{{\rm d}x{\rm d}Q^2}\left[1 - P_z P_B D A_1^{\rm d} + \frac{1}{2}P_{zz}A_{zz}^{\rm d}\right]. \quad (1)$$

Here, σ is the unpolarized cross section, $A_1^{\rm d}$ is the vector and $A_{zz}^{\rm d}$ the tensor asymmetry of the virtual-photon deuteron cross section, P_B is the beam polarization and D is the fraction of the beam polarization transferred to the virtual photon. In Eq. (1) and in the following Eq. (3), the fractional correction ($\lesssim 0.01$) arising from the interference between longitudinal and transverse photo-absorption amplitudes, which leads to the structure function g_2 [7], is neglected. Four independent polarized yields were measured (see Table I for the values of the achieved polarizations): $\sigma^{\overset{\rightarrow}{\Rightarrow}}$ and $\sigma^{\overset{\leftarrow}{\Rightarrow}}$ when the target spin is parallel and anti-parallel to that of the beam, respectively, $\sigma^{\Leftrightarrow}$ when the target has a mixture of helicity-1 states, and σ^0 when the target is in the helicity-0 state. The tensor asymmetry is extracted as

$$A_{zz}^{\rm d} = \frac{2\sigma^1 - 2\sigma^0}{3\sigma_U P_{zz}^{\rm eff}}, \quad (2)$$

where $\sigma^1 = (\sigma^{\overset{\leftarrow}{\Rightarrow}} + \sigma^{\overset{\rightarrow}{\Rightarrow}} + \sigma^{\Leftrightarrow})/3$ is the average over the helicity-1 states, $\sigma_U = (2\sigma^1 + \sigma^0)/3$ is the polarization-averaged yield and $P_{zz}^{\rm eff} = (P_{zz}^{\overset{\rightarrow}{\Rightarrow}} + P_{zz}^{\overset{\leftarrow}{\Rightarrow}} + P_{zz}^{\Leftrightarrow} - 3P_{zz}^{0})/9$ is the effective tensor polarization. In Eq. (2) the vector component due to $A_1^{\rm d}$ nearly cancels out: a residual vector polarization not more than 0.02 is achieved both for the σ^0, $\sigma^{\Leftrightarrow}$ and the averaged $(\sigma^{\overset{\leftarrow}{\Rightarrow}}+\sigma^{\overset{\rightarrow}{\Rightarrow}})/2$ measurements, (see Table I). Note that any contribution from residual vector polarization of the target is reduced to a negligible level by grouping together two sets of data with approximately the same statistics and opposite beam helicities.

The polarization-dependent structure function $g_1^{\rm d}$ can be extracted from the vector asymmetry $A_1^{\rm d}$ as

$$\frac{g_1^{\rm d}}{F_1^{\rm d}} \simeq A_1^{\rm d} \simeq \frac{c_{zz}}{|P_z P_B|D}\frac{(\sigma^{\overset{\leftarrow}{\Rightarrow}} - \sigma^{\overset{\rightarrow}{\Rightarrow}})}{(\sigma^{\overset{\leftarrow}{\Rightarrow}} + \sigma^{\overset{\rightarrow}{\Rightarrow}})}, \quad (3)$$

$$\text{with } c_{zz} = \frac{(\sigma^{\overset{\leftarrow}{\Rightarrow}} + \sigma^{\overset{\rightarrow}{\Rightarrow}})}{2\sigma_U} = 1 + \frac{(P_{zz}^{\overset{\leftarrow}{\Rightarrow}} + P_{zz}^{\overset{\rightarrow}{\Rightarrow}})}{4}A_{zz}^{\rm d}. \quad (4)$$

In all previous determinations of $g_1^{\rm d}$ the contribution of the tensor asymmetry $A_{zz}^{\rm d}$ was neglected, i.e. c_{zz} was assumed to be equal to 1, in spite of the fact that the vector polarization of the target could only be generated together with a non-zero tensor polarization. The present measurement quantifies the effect of $A_{zz}^{\rm d}$ on the existing $g_1^{\rm d}$ data.

For the determination of $A_{zz}^{\rm d}$, about 3.2 million inclusive events obtained with a tensor-polarized deuterium target are selected, by requiring as in the HERMES $g_1^{\rm d}$ analysis [8] a scattered positron with 0.1 GeV^2 $< Q^2 <$ 20 GeV^2 and an invariant mass of the virtual-photon nucleon system $W > 1.8$ GeV. The kinematic range covered by the selected data is $0.002 < x < 0.85$ and $0.1 < y < 0.91$, where y is the fraction of the beam energy carried by the virtual photon in the target rest frame. The asymmetry $A_{zz}^{\rm d}$ is calculated according to Eq. (2). The number of events determined per spin state is corrected for the e^+e^- background arising from charge symmetric processes (the latter is negligible at high x but amounts to almost 15% of the statistics in the lowest-x bin) and normalized to the luminosity measured by Bhabha scattering from the target gas electrons [4].

The asymmetry $A_{zz}^{\rm d}$ is corrected for detector smearing and QED radiative effects to obtain the Born asymmetry corresponding to pure single-photon exchange in the scattering process. The kinematic migration of the events

TABLE I: Hyperfine state composition, corresponding atomic population and polarization of the target states [6] employed in the $b_1^{\rm d}$ measurement as described in the text. The average target vector P_z and tensor P_{zz} polarizations are typically more than 80% of the ideal values. The average beam polarization $|P_B|$ is 0.53 ± 0.01. A positive P_B is assumed in the table. Four independent polarized yields, defined in the text, were measured depending on beam and target polarizations.

Target state	Hyper. state	Atomic popul.	Tensor term P_{zz}	Vector term $P_z \cdot P_B$	Meas. yield
vector$^+$	$\lvert 1\rangle + \lvert 6\rangle$	n^+	$+0.80 \pm 0.03$	$+0.45 \pm 0.02$	$\sigma^{\overset{\rightarrow}{\Rightarrow}}$
vector$^-$	$\lvert 3\rangle + \lvert 4\rangle$	n^-	$+0.85 \pm 0.03$	-0.45 ± 0.02	$\sigma^{\overset{\leftarrow}{\Rightarrow}}$
tensor$^+$	$\lvert 3\rangle + \lvert 6\rangle$	$n^+ + n^-$	$+0.89 \pm 0.03$	0.00 ± 0.01	$\sigma^{\Leftrightarrow}$
tensor$^-$	$\lvert 2\rangle + \lvert 5\rangle$	n^0	-1.65 ± 0.05	0.00 ± 0.01	σ^0

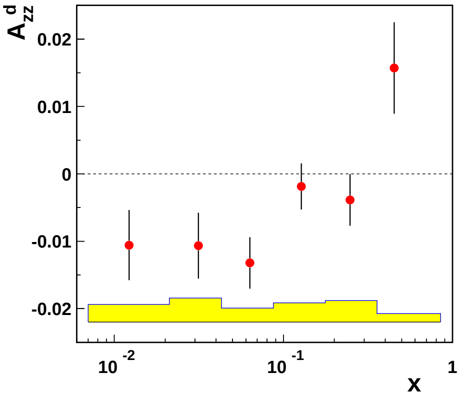

FIG. 1: The tensor asymmetry $A^{\rm d}_{zz}(x)$. The error bars are statistical and the shaded band shows the systematic uncertainty.

due to radiative and detector smearing is treated using an unfolding algorithm, which is only sensitive to the detector model, the known unpolarized cross section, and the models for the background processes [10]. The radiative background is negligible at high x but increases as $x \to 0$ and reaches almost 50 % of the statistics in the lowest-x bin. The radiative corrections are calculated using a Monte Carlo generator based on RADGEN [9]. The coherent and quasi-elastic radiative tails are estimated using parameterizations of the deuteron form factors [11, 12] and corrected for the tracking inefficiency due to showering of the radiated photons. The polarized part of the quasi-elastic radiative tail is neglected since there is no net tensor effect by inclusive scattering on weakly-bound spin-1/2 objects [13]. The extracted tensor asymmetry $A^{\rm d}_{zz}$ is shown in Fig. 1 and listed in Table II. It appears to be positive at high x and is negative at low x, crossing zero at an x value of about 0.2. In the lowest-x bin, the asymmetry is not zero at the 2-sigma level only after the subtraction of the radiative background. The magnitude of the observed tensor asymmetry $A^{\rm d}_{zz}$ does not exceed 0.02 over the measured range; from this result and using Eqs. (3) and (4), the fractional correction to the HERMES $g^{\rm d}_1$ measurement due to the tensor asymmetry is estimated to be less than 0.01.

The particle identification efficiency and the target polarization measurement give negligible contributions to the systematic uncertainty. The normalization uncertainty between different injection modes of the ABS is $\approx 1\times10^{-3}$ and correlated over the kinematic bins. This uncertainty is estimated by the observed 2-sigma offset from zero of the asymmetry between averaged vector, $2\sigma^1 = \sigma^{\Rrightarrow} + \sigma^{\Lleftarrow}$, and tensor$^+$, σ^0 replaced by $\sigma^{\Leftrightarrow}$ in Eq. (2), non-zero helicity injection modes. The luminosity measurement is sensitive to possible residual polarization of the target gas electrons. The asymmetries obtained by normalizing the yields to the luminosity-monitor rates, or to the beam-current times the target-gas analyzer rates, are in good agreement within the quoted normalization uncertainty. The subtraction of the radiative background inflates the size of the statistical and the above mentioned systematic uncertainties by almost a factor of 2 at low x. The systematic uncertainty of the radiative corrections is $\approx 2\times10^{-3}$ for the three bins at low x and negligible at high x. A possible misalignment in the spectrometer geometry yields an uncertainty $\approx 3\times10^{-3}$ in the bins where the asymmetry changes sign. All the contributions to the systematic uncertainty are added in quadrature. The two subsamples of data with opposite beam helicities were analyzed independently and gave consistent $A^{\rm d}_{zz}$ results.

The tensor structure function $b^{\rm d}_1$ is extracted from the tensor asymmetry using the relations [18, 27]

$$b^{\rm d}_1 = -\frac{3}{2}A^{\rm d}_{zz}\,F^{\rm d}_1 \;; \qquad F^{\rm d}_1 = \frac{(1+Q^2/\nu^2)F^{\rm d}_2}{2x(1+R)}. \quad (5)$$

No contribution from the hitherto unmeasured double spin-flip structure function Δ [14] is considered here, being kinematically suppressed for a longitudinally polarized target [15]. The structure function $F^{\rm d}_2$ is calculated as $F^{\rm d}_2 = F^{\rm p}_2(1+F^{\rm n}_2/F^{\rm p}_2)/2$ using the parameterizations of the precisely measured structure function $F^{\rm p}_2$ [16] and $F^{\rm n}_2/F^{\rm p}_2$ ratio [17]. In Eq. (5), $R=\sigma_L/\sigma_T$ is the ratio of longitudinal to transverse photo-absorption cross sections [18] and ν is the virtual-photon energy. The results for $b^{\rm d}_1$ are listed together with those for $A^{\rm d}_{zz}$ in Table II. The x-dependence of $b^{\rm d}_1$ is displayed in Fig. 2. The data show that $b^{\rm d}_1$ is different from zero for $x<0.1$, its magnitude rises for decreasing values of x and, for $x \lesssim 0.03$, becomes even larger than that of $g^{\rm d}_1$ at the same value of Q^2 [8].

Because the deuteron is a weakly-bound state of spin-1/2 nucleons, $b^{\rm d}_1$ was initially predicted to be negligible, at least at moderate and large values of x ($x>0.2$) [19, 20], where it should be driven by nuclear binding and Fermi motion effects. It was later realized that $b^{\rm d}_1$ could rise to values which significantly differ from zero as $x\to0$, and its magnitude could reach about 1% of the unpolarized structure function $F^{\rm d}_1$, due to the same mechanism that leads to the well known effect of nuclear shadowing in unpolarized scattering [21].

TABLE II: Measured values (in 10^{-2} units) of the tensor asymmetry $A^{\rm d}_{zz}$ and the tensor structure function $b^{\rm d}_1$. Both the corresponding statistical and systematic uncertainties are listed as well.

$\langle x\rangle$	$\langle Q^2\rangle$ [GeV^2]	$A^{\rm d}_{zz}$ [10^{-2}]	$\pm\delta\mathcal{A}^{\rm stat}_{zz}$ [10^{-2}]	$\pm\delta\mathcal{A}^{\rm sys}_{zz}$ [10^{-2}]	$b^{\rm d}_1$ [10^{-2}]	$\pm\delta b_1^{\rm stat}$ [10^{-2}]	$\pm\delta b_1^{\rm sys}$ [10^{-2}]
0.012	0.51	-1.06	0.52	0.26	11.20	5.51	2.77
0.032	1.06	-1.07	0.49	0.36	5.50	2.53	1.84
0.063	1.65	-1.32	0.38	0.21	3.82	1.11	0.60
0.128	2.33	-0.19	0.34	0.29	0.29	0.53	0.44
0.248	3.11	-0.39	0.39	0.32	0.29	0.28	0.24
0.452	4.69	1.57	0.68	0.13	-0.38	0.16	0.03

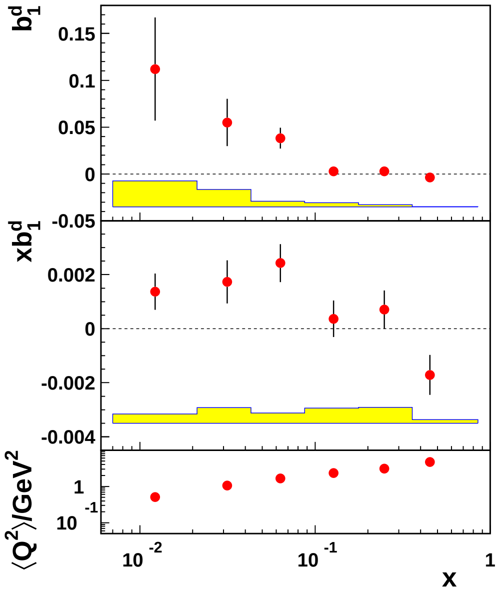

FIG. 2: The tensor structure function presented as (top) $b_1^{\rm d}(x)$ and (middle) $xb_1^{\rm d}(x)$. The error bars are statistical and the shaded bands show the systematic uncertainty. The bottom panel shows the average value of Q^2 in each x-bin.

This feature is described by coherent double-scattering models [22–28]. The observed $b_1^{\rm d}$ confirms qualitatively the double-scattering model predictions, except for the negative value at $\langle x\rangle = 0.452$, which, however, is still compatible with zero at the 2-sigma level. In the context of the Quark-Parton Model description, the sum rule $\int b_1(x){\rm d}x = 0$ is broken if the quark sea is tensor polarized [29, 30]. From the x-behavior of $xb_1^{\rm d}$ shown in Fig. 2 it can be seen that the first moment of $b_1^{\rm d}$ is non-zero. A 2-sigma result, $\int_{0.002}^{0.85} b_1(x){\rm d}x = (1.05 \pm 0.34\,_{\rm stat} \pm 0.35\,_{\rm sys}) \cdot 10^{-2}$, is obtained within the measured range, and a 1.7-sigma result, $\int_{0.02}^{0.85} b_1(x){\rm d}x = (0.35 \pm 0.10\,_{\rm stat} \pm 0.18\,_{\rm sys}) \cdot 10^{-2}$, within the restricted x-range where $Q^2 > 1$ GeV^2. The integrals are calculated after having $b_1^{\rm d}$ evolved to $Q_0^2 = 5$ GeV^2 by assuming a Q^2-independence of the measured $b_1^{\rm d}/F_1^{\rm d}$ ratio, $b_1^{\rm d}(Q_0^2) = b_1^{\rm d}/F_1^{\rm d} \cdot F_1^{\rm d}(Q_0^2)$.

In conclusion, HERMES has provided the first measurement of the tensor structure function $b_1^{\rm d}$, in the kinematic domain $0.01 < \langle x\rangle < 0.45$ and 0.5 GeV$^2 < \langle Q^2\rangle < 5$ GeV^2. The function $b_1^{\rm d}$ is found to be different from zero for $x < 0.1$. Its first moment is found to be not zero at the 2-sigma level within the measured x range. The $b_1^{\rm d}$ measurement can be used to reduce the systematic uncertainty on the $g_1^{\rm d}$ measurement that is assigned to the tensor structure of the deuteron. The behavior of $b_1^{\rm d}$ at low values of x is in qualitative agreement with expectations based on coherent double-scattering models.

We gratefully acknowledge the DESY management for its support, the staff at DESY and the collaborating institutions for their significant effort, and our national funding agencies for financial support. We are grateful to N. Nikolaev and O. Shekhovtsova for useful discussions.

[1] P. Hoodbhoy *et al.*, Nucl. Phys. B **312**, 571 (1989).
[2] A. Pais, Phys. Rev. Lett. **19**, 544 (1967).
[3] L. L. Frankfurt *et al.*, Nucl. Phys. A **405**, 557 (1983).
[4] HERMES Coll., K. Ackerstaff *et al.*, Nucl. Instr. Meth. A **417**, 230 (1998).
[5] A. Sokolov and L. Ternov, Sov. Phys. Doklady **8**, 1203 (1964).
[6] HERMES Coll., A. Airapetian *et al.*, Nucl. Instr. Meth. A **540**, 68 (2005).
[7] E155 Coll., P. L. Anthony *et al.*, Phys. Lett. B **553**, 18 (2003).
[8] HERMES Coll., $g1$ paper, in preparation. C. Riedl, in *Proc. of 16th International Spin Physics Symposium*, Trieste 2004, hep-ex/0411087. C. Riedl, PhD–thesis.
[9] I. V. Akushevich *et al.*, hep-ph/9906408.
[10] HERMES Coll., A. Airapetian *et al.*, Phys. Rev. D **71**, 012003 (2005).
[11] D. Abbott *et al.*, Eur. Phys. J. A **7**, 421 (2000).
[12] S. Stein *et al.*, Phys. Rev. **12**, 1884 (1975).
[13] Z.-L. Zhou *et al.*, Phys. Rev. Lett. **82**, 687 (1999).
[14] R. L. Jaffe *et al.*, Phys. Lett. B **223**, 218 (1989).
[15] E. Sather *et al.*, Phys. Rev. D **42**, 1424 (1990).
[16] H. Abramowicz *et al.*, hep-ph/9712415.
[17] NMC, P. Amaudruz *et al.*, Nucl. Phys. B **371**, 3 (1992).
[18] L. W. Whitlow *et al.*, Phys. Lett. B **250**, 193 (1990).
[19] H. Khan *et al.*, Phys. Rev. C **44**, 1219 (1991).
[20] A. Yu. Umnikov, Phys. Lett. B **391**, 177 (1997).
[21] EMC, J. Ashman *et al.*, Phys. Lett. B **206**, 364 (1988).
[22] G. A. Miller, in *Electronuclear Physics with Internal Targets*, ed. R. G. Arnold (World Scientific, Singapore, 1989), p.30.
[23] H. Khan *et al.*, Phys. Lett. B **298**, 181 (1993).
[24] M. Strikman, in *Proceedings of the Symposium on Spin Structure of the Nucleon*, ed. V. H. Hughes and C. Cavata (World Scientific, Singapore, 1995), p.153.
[25] N. N. Nikolaev *et al.*, Phys. Lett. B **398**, 245 (1997).
[26] J. Edelmann *et al.*, Z. Phys. A **357**, 129 (1997).
[27] J. Edelmann *et al.*, Phys. Rev. C **57**, 3392 (1998).
[28] K. Bora *et al.*, Phys. Rev. D **57**, 6906 (1998).
[29] F. E. Close *et al.*, Phys. Rev. D **42**, 2377 (1990).
[30] A. V. Efremov *et al.*, Sov. J. Nucl. Phys. **36**, 557 (1982).